ISSN 1990-3413, Astrophysical Bulletin, 2024, Vol. 79, No. 2, pp. 321–339. © Pleiades Publishing, Ltd., 2024.
Original Russian Text © The Author(s), 2024, published in Astrofizicheskii Byulleten', 2024, Vol. 79, No. 2, pp. 331–349.

Prospects of Millimeter Astronomy Development at the Special Astrophysical Observatory of the Russian Academy of Sciences (SAO RAS)

V. A. Stolyarov[1*], Y. Y. Balega[1,2], M. G. Mingaliev[1,3,4], Y. V. Sotnikova[1,3], V. F. Vdovin[5,1], A. A. Gunbina[5], D. E. Kukushkin[1,6], M. A. Tarasov[7], M. Y. Fominsky[7], A. M. Chekushkin[7], V. S. Edelman[8], and R. A. Yusupov[7]

[1]*Special Astrophysical Observatory, Russian Academy of Sciences, Nizhnii Arkhyz, 369167 Russia*
[2]*China Branch of BRICS Institute of Future Networks, Shenzhen, 518000 China*
[3]*Kazan (Volga Region) Federal University, Kazan, 420008 Russia*
[4]*Institute of Applied Astronomy, Russian Academy of Sciences, St. Petersburg, 191187 Russia*
[5]*Federal research center A. V. Gaponov-Grekhov Institute of Applied Physics of the Russian Academy of Sciences, Nizhny Novgorod, 603950 Russia*
[6]*ITMO University, St. Petersburg, 197101 Russia*
[7]*Kotelnikov Institute of Radioengineering and Electronics of Russian Academy of Sciences, Moscow, 125009 Russia*
[8]*P. L. Kapitza Institute for Physical Problems Russian Academy of Sciences, Moscow, 119334 Russia*
Received October 30, 2023; revised March 18, 2024; accepted March 18, 2024

Abstract—The article discusses the prospects for developing the observational base at the Special Astrophysical Observatory of the Russian Academy of Sciences (SAO RAS) for astrophysical research in the millimeter-wave range. As a first step, a project is proposed to create a set of sub-terahertz receiving equipment to operate at the optical BTA telescope. Additionally, the possibility of installing a new instrument to operate in the frequency range of up to 230 GHz ($\lambda = 1.3$ mm) at the Upper Research Site of SAO RAS is considered. Technical and operational characteristics of the instrument, site selection for the installation of a fully steerable millimeter-wave antenna, statistics of meteorological data and atmospheric absorption are discussed. A list of potential scientific tasks addressed by instruments of this class is provided.

DOI: 10.1134/S1990341324600467

Keywords: *atmospheric effects—instrumentation: detectors—instrumentation: interferometers—methods: observational*

1. INTRODUCTION

Research in the field of millimeter and submillimeter[1)] astronomy has started relatively recently but has already yielded significant scientific results (see, for example, Boccardi et al., 2017; Akiyama et al., 2019; Eklund et al., 2020; Guélin and Cernicharo, 2022). Measurements in this band require excellent weather conditions, sensitive receivers, and highly accurate antennas. Across the world, there are a small number of telescopes of this type, both individual antennas, such as the 30-m IRAM antenna in Spain (Sánchez-Portal, 2023), SRT in Sardinia (Prandoni et al., 2017), LMT in Mexico (Hughes et al., 2020), the 45-m radio telescope at NRO (Japan, Hirabayashi, 1985), and interferometers, such as, ALMA (Chile, Dougherty, 2020), NOEMA (France, Schuster et al., 2018), ATCA (Australia, Indermuehle and Burton, 2014), KVN (South Korea, Chol Minh et al., 2004). In Russia, this group of instruments includes three RT-13 antennas (Institute of Applied Radio Astronomy of the Russian Academy of Sciences (IAR RAS), Shuygina et al., 2019) with a diameter of 13.2 m, which operate in the frequency range up to 40 GHz and are used almost exclusively for applied

*E-mail: vlad@sao.ru

1)According to the classification by the International Telecommunication Union (ITU), the range with $\lambda = 1-10$ mm corresponds to the millimeter-wave region, while the range with $\lambda = 0.1-1$ mm corresponds to the submillimeter-wave region.

purposes. Unfortunately, there are currently no instruments for astronomical observations in Russia in the millimeter and submillimeter ranges at frequencies above 100 GHz. This lack of equipment poses challenges for russian scientists in addressing numerous scientific tasks in these frequency bands.

On the other hand, participation in large international projects, such as the Event Horizon Telescope (EHT, Akiyama et al., 2019) or Millimetron (Novikov et al., 2021), requires not only the availability of the appropriate instrument but also experience in conducting observations in the millimeter range. This experience can be obtained with a relatively small telescope installed at the observing site among other instruments, where the necessary infrastructure and engineering support are already in place.

The list of tasks that can be addressed with an instrument of this class is quite extensive. In single-dish mode, one can mention surveys of the visible part of the celestial sphere in molecular lines of CO $J = 1-0$ (115 GHz) and CO $J = 2-1$ (230 GHz), construction of maps of extragalactic sources in molecular lines, monitoring of active galactic nuclei (AGNs) in collaboration with the main instruments of the SAO RAS, the radio telescope RATAN-600[2)] (Parijskij, 1993) and the optical telescope BTA[3)] (Ioannisiani et al., 1982); investigation of the Sunyaev–Zeldovich effect in galaxy clusters, projects for searching for lines of complex molecules in the interstellar medium, and other tasks.

Furthermore, such an instrument can be used in the Very Long Baseline Interferometry (VLBI) mode in projects like "Suffa" (Hojaev et al., 2007) and EHT, as well as as a component of the "Earth–Space" interferometer in collaboration with the "Millimetron."

If a project is implemented quickly, the instrument can be put into operation within 5–6 years. As practice shows, the lifespan of large radio astronomical instruments exceeds half a century. For example, 30-m IRAM antenna was built in the 1980s and has been in use for almost 40 years. RATAN-600 telescope, which remains the main instrument of the Special Astrophysical Observatory of the Russian Academy of Sciences, was commissioned in December 1976. It is expected that the SKA interferometer (Dewdney et al., 2009), which will use antennas manufactured by CETC54 (China), will operate for 50–60 years after its construction is completed.

[2)]https://rat.sao.ru/en/telescope/

[3)]https://www.sao.ru/Doc-en/Telescopes/bta/descrip.html

2. THE SUBTERAHERTZ OBSERVATORY PROJECT AS PART OF THE BTA OPTICAL TELESCOPE

The proposals for testing the subterahertz range receiving equipment on the 6-m BTA optical telescope emerged in the mid-2000s. At that time, some preliminary work was carried out on the fabrication of radiation detectors. Currently, the implementation of a similar project has commenced, but now on a new component basis, taking into account the progress in the field of terahertz electronics over the past decade and a half.

2.1. The Concept of a Subterahertz Observatory as Part of the BTA

The main idea has not undergone significant changes and is described in the work by Vystavkin et al. (2008). At the Nasmyth-1 focus of the BTA telescope it is planned to install and test various subterahertz receivers for observations in the frequency range from 86 to 380 GHz (wavelength range of 3.4–0.8 mm), utilizing atmospheric transparency windows. The technology chosen for the detectors is superconductor–insulator–normal metal–insulator–superconductor (SINIS) (Balega et al., 2020; Tarasov et al., 2022). A corrective optics system will be used to align the detectors with the telescope's optical scheme. Additionally, a readout electronics system will be developed, and a cryostat will be manufactured to cool the detectors to a temperature no greater than 0.1 K. Initially, it was proposed to consider a prototype of the cryostat system based on the product presented by Edelman (2012). Currently, several designs of cryostat systems are being considered, and this issue is thoroughly discussed by Balega et al. (2023) (see Section 3).

The optical scheme of the BTA telescope is presented in Fig. 1a, taken from the work of Vystavkin et al. (2008). The primary mirror of the telescope with a diameter of 6 m (*1*) concentrates the incoming radiation at the primary focus (*2*). Near the primary focus is the secondary mirror (*5*), which forms a narrow beam propagating backward along the optical axis and impinging on the flat diagonal mirror (*4*), deflecting the beam by 90°. Then, the beam passes through a metallic tube (*3*) into the cabin (*6*). The focus Nasmyth-1 is located inside the cabin (*6*), where the receivers will be positioned.

It is necessary to note that the wavelengths in the sub-terahertz range are quite large, and the size of Airy disks will vary approximately from 60 mm for $\lambda = 0.8$ mm to 260 mm for $\lambda = 3.4$ mm. Therefore, the initial test observations with SINIS detectors at the BTA telescope site are planned to be conducted in

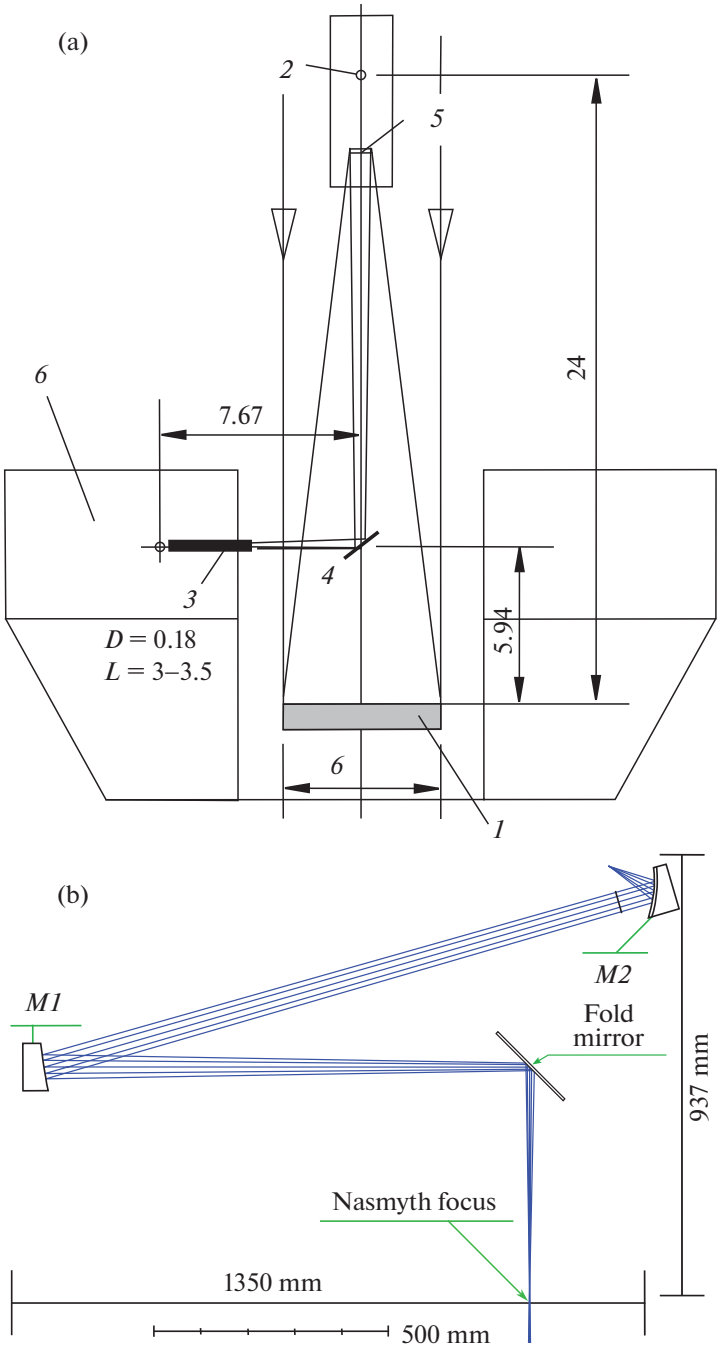

Fig. 1. Panel (a) the optical scheme of the BTA telescope (taken from the work by Vystavkin et al. (2008) with permission from the authors): (*1*) the primary mirror, (*2*) the main (primary) focus, (*3*) tube leading to Nasmyth-1, (*4*) the flat diagonal mirror deflecting the beam towards the Nasmyth-1 focus, (*5*) the secondary mirror, (*6*) the cabin with reception equipment. Dimensions are given in meters. Panel (b) the optical system of corrective optics with the following parameters: $f'_{M1} = 1250$ mm, $f'_{M2} = 100$ mm, linear magnification of the system $V = 0.08^{x}$.

single-pixel mode. Multi-pixel system can be considered for the future perspective.

At the moment, the issue of matching the signal collected by the telescope mirror with the detecting cell is at the stage of elaboration. Below are the current results of the work.

An assessment of the diameter of the telescope's diffraction spot at the Nasmyth focus was already performed (modeling results are presented in Balega et al., 2024). Paraxial characteristics of corrective optics were determined for signal matching. The relative aperture of the telescope at the Nasmyth

focus is 1/30, corresponding to the diameter of the first diffraction maximum for $\lambda = 2998$ μm $D_{\max} \approx$ 200 mm. Calculations of the matching optics showed that the optimal diameter of the horn, installed with the detecting cell inside the cryostat, is 20 mm. A back-to-back horn antenna was proposed and modeled as an antenna design. The results are presented in Balega et al. (2024). Therefore, the linear magnification of the optical system consisting of two paraboloids should not exceed $V = f'_2/f'_1 = 0.1^x$. The use of off-axis paraboloids will simplify the mirror installation along the reference optical path, as spherical aberration is neutralized. The main limitation on the maximum achievable magnification of the coordinating optics is the size of the platform at the Nasmyth focus and the structural features of the receiver. As a result, an optical system of corrective optics was developed (see Fig. 1b).

The system comprises two off-axis paraboloids, *M1* and *M2* with focal lengths $f'_{M1} = 1250$ mm, $f'_{M2} = 100$ mm and a flat mirror (Fold mirror). The linear magnification of the system is $V = 0.08^x$. After the corrective optics system, the diameter of the first diffraction maximum at $\lambda = 1303$ μm ($\nu =$ 230 GHz) was approximately $D_{\max} \approx 8$ mm, and at $\lambda = 2998$ μm ($\nu = 100$ GHz) $D_{\max} \approx 18.4$ mm, which does not exceed the diameter of the horn in front of the THz radiation receiver.

2.2. Prototype of Direct Detection Receiver

As a prototype for the direct detection receiver module, it is proposed to use SINIS detectors. A schematic diagram of a SINIS detector is shown in Fig. 2, with detailed descriptions available in the publications by Tarasov et al. (2022), Gunbina et al. (2021) and Tarasov et al. (2021). The sensitive element of such a detector is a nano-sized absorber made of normal metal. The heating of the absorber is proportional to the power of the incident radiation, which is measured by two tunnel junctions of the SIN structure (superconductor–insulator–normal metal). Depending on the topology of the SINIS structure, a detector with high quantum efficiency can be implemented. For example, in the work by Yusupov et al. (2020), a quantum efficiency of 15 electrons per photon was measured for a SINIS detector at a frequency of 350 GHz. The detector itself is not selective in terms of frequency and polarization of radiation; the frequency and bandwidth of reception are determined by planar antennas into which individual SINIS detectors and filtering elements are integrated in the measurement path.

In the development of the receiving system as part of an observatory, an important factor is the background load, which can be on the order of tens of picowatts under conditions of operation in a ground-based instrument. A single SINIS detector saturates at a power level of about 0.5–1.0 pW. When combining such detectors into arrays, the incoming radiation is distributed among them, allowing for the adjustment of the desired saturation level. Due to the compactness of the detector (sizes up to 10×5 μm or less, depending on the requirements of the topology and the technology used), up to four detectors can be integrated into one antenna. It is assumed that microwave readout systems based on superconducting coplanar resonators will be used for matrix detectors. The first results of test studies with such a readout system with SINIS detectors are presented in the work by Gunbina et al. (2021). Photographs of some manufactured arrays are shown in Fig. 3. Expected and preliminarily measured characteristics of sensitivity for various SINIS detector arrays in laboratory conditions are as follows:

- volt-watt sensitivity up to 10^{10} V W^{-1};
- noise equivalent power (NEP) no worse than 10^{-16} W Hz$^{-1/2}$;
- fluctuational sensitivity of 100 μK Hz$^{-1/2}$ at a temperature of 2.7 K (Tarasov et al., 2020).

To calculate the sensitivity of the receiving system taking into account the characteristics of the BTA telescope, one can utilize the concept of Noise Equivalent Flux Density (Noise Equivalent Flux Density (NEFD), Leclercq, 2017). Preliminary estimates show that with the given NEP value and a bandwidth of approximately 10% of the central frequency $\nu_c =$ 100 GHz and an aperture efficiency of $\eta_A \approx 0.8$, this parameter will be NEFD ≈ 100 mJy Hz$^{-1/2}$. In this case, an object with a flux density of $S_\nu = 10$ mJy with $S/N \approx 5$ can be observed with an integration time of 30–40 minutes.

A significant feature of highly sensitive receivers for terahertz astronomy is the necessity for deep cryogenic cooling, requiring the creation of vacuum cryostats and various interfaces (optical, electrical, mechanical, thermal, etc.) to ensure efficient operation.

Another key interface of such receiving systems is the quasi-optical path, which matches the signal collected by the giant telescope mirror with the nano-sized detector. In addition to matching and correcting elements of the receiving path, the following issues can also be highlighted: the vacuum window in the cryostat (its material and dimensions); radiation filters to suppress parasitic background radiation; matching elements inside the cryostat, and so on. Some matching and filtering elements that were used in laboratory experiments to study the characteristics of receiving arrays based on SINIS detectors, are presented in the works of Tarasov et al. (2020, 2022).

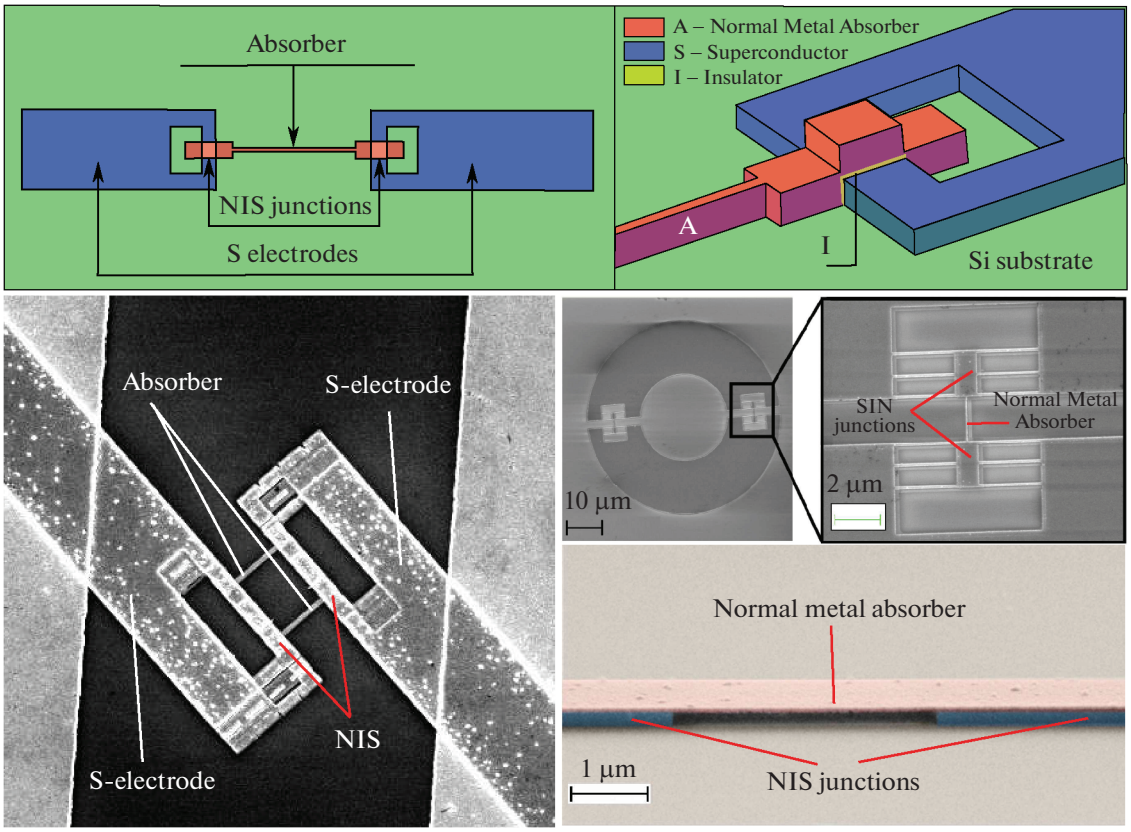

Fig. 2. SINIS detector: (a) schematic representation of a SINIS detector; (b) photographs taken with a scanning electron microscope of SINIS detectors of various topologies. Photographs from the publication by Gunbina et al. (2021).

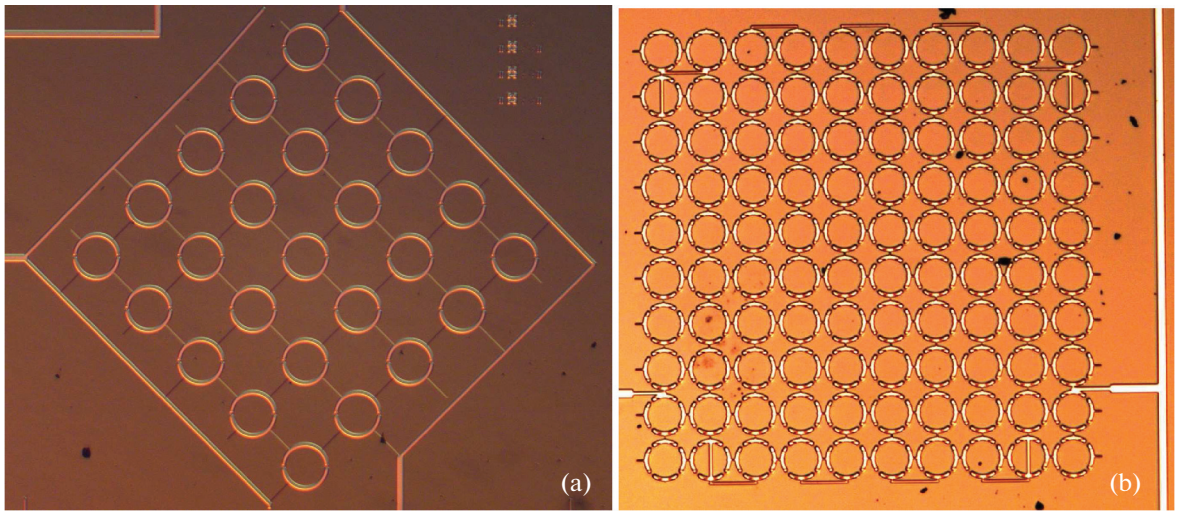

Fig. 3. Arrays of planar antennas for the 350 GHz: (a) half-wave antennas, (b) electrically small antennas.

Another element of such systems contributing to noise (and consequently, to the overall sensitivity of the system) is the readout electronics. One option for signal readout—"warm" (operating at room temperature) electronics based on operational amplifiers (JFET or MOSFET transistors). The main drawback of such a system is its relatively high intrinsic noise of 20 nV $Hz^{-1/2}$. This does not pose problems for ground-based measurements, as the requirements for noise equivalent power (NEP) do not exceed values of 10^{-16} W $Hz^{-1/2}$. This level is sufficient for observations under conditions of high

background load. This parameter in ground-based observations is mainly determined by the high values of atmospheric temperature $T_{\rm atm}$ and radiation from the "warm" ground entering the receiving path due to the side lobes of the antenna. However, for more sensitive observations on balloon-borne telescopes, and especially for space missions, it is necessary to reduce the noise of the readout electronics. This is also important for multi-pixel systems, where a large number of readout electronics wires can introduce a significant level of noise. A promising approach is the use of microwave readout electronics based on high-Q superconducting coplanar resonators with a cold HEMT[4)] amplifier (the first results of integrating SINIS detectors into such a system are presented in the work by Gunbina et al., 2021) with the further prospect of integrating Josephson parametric amplifiers on-chip. Information on the progress of the project to install SINIS detectors at the BTA telescope site is provided in the work by Balega et al. (2024).

3. CHARACTERISTICS OF A SPECIALIZED INSTRUMENT FOR OBSERVATIONS IN THE MILLIMETER BAND

The project of a subterahertz observatory as part of the Special Astrophysical Observatory of the Russian Academy of Sciences (SAO RAS), currently underway, is primarily intended for testing receiving equipment in this band and cannot be a long-term solution. For organizing observations in the millimeter and submillimeter bands at SAO RAS on a permanent basis, it is necessary to create a specialized instrument based on a fully steerable antenna of the reflector type.

Let's briefly consider the main requirements for this instrument, the possible characteristics of which are given in Table 1. When calculating the system equivalent flux density (SEFD), estimates of the receiver noise temperature $T_{\rm rec}$, atmospheric temperature $T_{\rm atm}$ and stray radiation due to antenna side lobes $T_{\rm spur}$ were used, similar to the estimates made in the ALMA memorandum (Magnum, 2017). It is worth noting that the characteristics presented in Table 1 are quite conservative, and the instrument's efficiency can be improved, for example, by increasing the aperture efficiency η_A, which for ALMA antennas is 0.7–0.8 at frequencies up to 300 GHz.

The SEFD values given in Table 1 refer to the receiver input and do not account for signal attenuation in the atmosphere, but they are sufficient for conducting subsequent assessments.

[4)]High Electron Mobility Transistor, a type of a field-effect transistor.

3.1. Antenna Parameters

Taking into account several factors, primarily meteorological conditions, the optimal solution appears to be installing an antenna for observations in the millimeter band across three spectral windows from $\nu_c = 100$ GHz ($\lambda = 3$ mm) to $\nu_c = 230$ GHz ($\lambda = 1.3$ mm), corresponding to atmospheric transparency windows. A reasonable compromise between cost, weather conditions, and diversity of scientific tasks could be a fully steerable antenna of small diameter (up to 15 m) with a primary mirror surface accuracy of approximately 55 μm. The standard optical scheme commonly employed in such instruments (like ALMA, NOEMA) is the Cassegrain scheme.

3.1.1. Possible antenna options. Since astronomical instruments of this class are unique installations, there are very few manufacturers of antennas for millimeter observations worldwide. Among them, notable companies include EIE[5)] and Vertex[6)]. Additionally, there are companies in Southeast Asia and China that develop and manufacture such instruments, such as CETC 54[7)], subcontractors like those involved in the SKA-MID project (Pellegrini et al., 2021). In some cases, astronomical institutions handle the manufacturing and installation of antennas themselves through subcontractors, as seen with IRAM and the NOEMA interferometer. Some antenna options are provided for illustration in Fig. 4.

Depending on the weather conditions, the antenna is sometimes housed in a radio-transparent dome, which increases the overall cost of the structure. The decision to use such a dome should be made after studying the astroclimate at the telescope's installation site.

3.2. Receiving Equipment

It is assumed that the instrument will be equipped with polarization receivers for observations across a wide frequency range from 86 to 260 GHz. For operation in the frequency range of the first spectral window from 86 to 116 GHz it is justified to use receivers based on HEMT amplifiers, manufactured as monolithic microwave integrated circuit (MMIC). There are numerous developments of receiving equipment based on HEMT in this range. In particular, one can note the development of such receivers for ALMA project (Yagoubov et al., 2020).

The task of operating within the Very Large Base Interferometer (VLBI) network precludes the use of

[5)]http://www.eie.it/en
[6)]https://www.vertexant.com/
[7)]http://www.militram.com/cetc-54-antenna-capability-products/

Fig. 4. Options of antennas for installation: (a) EIE antenna, credit: ALMA (ESO/NAOJ/NRAO); (b) Vertex antenna, credit: ALMA (ESO/NAOJ/NRAO); (c) NOEMA interferometer antenna, credit: NOEMA (IRAM).

the bolometers as detectors for the second and third spectral windows at frequencies from 140 to 260 GHz because the phase component of the signal would be lost in this case. Standard practice for observations in the millimeter band at frequencies above 120–150 GHz and up to terahertz involves the use of coherent (heterodyne) receivers with SIS mixers[8] (Wilson and Guilloteau, 2018).

Currently, significant progress is being made worldwide, including in Russia, in the field of low-noise SIS receivers, particularly in connection with the start of the "Millimetron" project (Novikov et al., 2021). For example, Rudakov et al. (2020) examined a low-noise SIS receiver designed to operate in the 211–275 GHz range, developed by researchers from Kotelnikov Institute of Radioengineering and Electronics (IRE) of Russian Academy of Sciences in collaboration with colleagues from the Astronomical Institute of the University of Groningen (Netherlands). This receiver is intended for use in both space-based instruments and ground-based projects. A similar receiver could be installed on the proposed millimeter telescope of the Special Astrophysical Observatory of the Russian Academy of Sciences.

It is easy to estimate that with the stated values of the SEFD in Table 1 with a bandwidth of 4 and 8 GHz for the central frequency $\nu_c = 100$ and 230 GHz respectively, and with a half-hour integration time, the sources with flux densities of approximately 10–20 mJy can be observed with a signal-to-noise ratio $S/N \approx 5$, depending on the zenith angle.

It is also worth noting that for single-dish mode, kinetic inductance detectors (KID) have been developed. In particular, the NIKA-2 instrument is equipped with an array of such detectors on the 30-m telescope at IRAM in Spain (Adam et al., 2018). This camera, with three thousand pixels covering two bands at 150 and 260 GHz, allows for a field of view of up to 6′.5 with a resolution of 17″.5 and 11″ at these frequencies.

Receiving horns for different frequency ranges are typically installed on interchangeable cartridges or on a rotating drum-type platform in the focal area of the antenna.

For signal digitization, spectrum acquisition, and conversion of digitized signals into VLBI data format (Mark6), a design by the CASPER[9] collaboration can be used: Roach-2 based on a field-programmable gate array (FPGA) Xilinx Virtex-6 (Kubo et al., 2018).

4. SITE SELECTION AND ESTIMATION OF WATER CONTENT IN THE ATMOSPHERE

There are three obvious locations where an antenna can be installed without significant costs for creating new infrastructure on the land of the SAO RAS. These are the territory of the RATAN-600 near the Zelenchukskaya place (altitude 974 m), the Upper Research Site (URS, altitude 2070 m) and a point 1.5 km southeast of the URS, known as the Semirodniki Hill (altitude 2340 m). The first two locations

[8] Superconductor—Insulator—Superconductor.

[9] https://casper.berkeley.edu/

Table 1. Technical specifications

Instrument type	Fully steerable antenna
The type of antenna	The Cassegrain scheme
The diameter of the primary mirror, m	15
The aperture efficiency across all frequency ranges η_A	>0.65
Frequency ranges, GHz	86–116, 140–165, 200–260
Surface accuracy, micrometers	55
Pointing accuracy, arcsec	2
Tracking accuracy, arcsec	0.3
Equivalent flux density of the SEFD system, Jansky	–
SEFD ($\nu = 100$ GHz, $T_{\rm rec} = 40$ K, $T_{\rm atm} = 30$ K, $T_{\rm spur} = 20$ K)	2200
SEFD ($\nu = 230$ GHz, $T_{\rm rec} = 40$ K, $T_{\rm atm} = 80$ K, $T_{\rm spur} = 20$ K)	3400
Bandwidth, GHz	up to 8 (for SIS mixer)
Number of spectral channels	up to 32 768
Type of receivers ($\nu = 86$–116 GHz)	HEMT, cryogenic
Type of receivers ($\nu > 140$ GHz)	SIS, cryogenic
Maximum resolution, arcsec	20

have sufficiently long series of meteorological parameters, while for the third location, it is necessary to perform their monitoring.

In addition to monitoring meteorological parameters at any site before installing an antenna, it is required to conduct engineering-geological surveys. The tasks of these surveys include comprehensive study of the engineering-geological conditions to obtain necessary and sufficient materials for the development of construction documentation for service premises and the antenna itself. This includes studying the terrain relief, geological structure, geomorphological and hydrogeological conditions, composition, condition, and properties of soils, geological and engineering-geological processes. Furthermore, it involves making forecasts for possible changes in engineering-geological conditions in the interaction of the designed objects with the geological environment.

4.1. The Methodology for Estimating Precipitated Water Content Based on Meteorological Data

Knowing the air temperature and relative humidity, it is possible to estimate the precipitated water content in millimeters (perceptible water vapor, PWV, water vapor content in the unit cross-section air column) using the methodology described by Otárola (2010):

$$e_0 = e_s \frac{\rm RH}{100},$$

$$e_s = 611.21 \exp\left[\left(18.68 - \frac{T}{234.5}\right)\left(\frac{T}{257.1 + T}\right)\right],$$

$$\rho_{V_0} = \frac{e_0}{R_V T({\rm K})},$$

$$\mathrm{PWV} = 1000\, H\, \rho_{V_0}\left(1 - \exp\left(\frac{z_0 - z_{\max}}{H}\right)\right),$$

where e_0—the partial pressure of water vapor at the surface in pascals; e_s—the partial pressure of water vapor at saturation as a function of air temperature T (in degrees Celsius) at the surface; RH—the relative humidity of air at the surface in percentage; ρ_{V_0}—the density of water vapor at the surface (kg m^{-3}); $R_V = 461.9$ —the gas constant for water vapor (J kg^{-1} K^{-1}); T(K)—the air temperature in degrees Kelvin; H—the characteristic scale for water vapor in kilometers, for these calculations, is taken as 1.68 km; z_0—the geographical altitude of the location in kilometers; $z_{\max}$—the maximum altitude, up to which the integration of the water vapor profile was conducted, is taken as 12 km.

4.2. Meteorological Data Statistics and PWV Estimation for the Upper Research Site

The Upper Research Site (URS) of the SAO RAS is the most convenient location for placing a millimeter telescope. It houses the main optical instruments—such as the 6-m BTA telescope, the Zeiss-1000 with a 1-m mirror, and several smaller instruments. The site elevation is 2070 meters above sea level. Since the water content in the atmospheric column depends on altitude, this value is lower at the URS compared to lower-lying places, such as the RATAN-600. Figures 5a,b,c show: the histogram of the distribution of PWV values in millimeters for the entire observation period from 2008 to 2020; the averaged PWV values by month, including daily, daytime, and nighttime values; and the empirical cumulative distribution function (CDF) for PWV values. From the graphs, it can be seen that PWV $<$ 5 mm occurs in 30% of cases, and PWV $<$ 7 mm occurs in half of the cases, corresponding to the six-month period from October to April.

Figure 5d shows the histogram of the distribution of wind gust speeds for the entire observation period (2008–2020). Despite the fact that wind loads on the URS are greater than on the plain, during the observation period, wind gust speeds reached 40 m s^{-1} only once. Although operational conditions differ for antenna structures from different manufacturers, observations in normal mode are usually conducted at an average wind speed of less than 10–12 m s^{-1} (with gusts less than 15 m s^{-1}). Further work on certain tasks is possible at an average wind speed of less than 22 m s^{-1}, above which the antenna is stowed, minimizing the aerodynamic resistance of the structure. The survival wind speed limit (survival conditions at stow) for most antennas typically ranges from 50 to 55 m s^{-1}.

4.3. Option for Antenna Installation on Semirodniki Hill

In the southeast direction from the URS, at a distance of 1.5 km lies Semirodniki Hill, with an elevation of 2340 m, which is 250 m higher than the location of the main optical instruments of the SAO RAS (Fig. 6). Currently, there is no meteorological monitoring data available for this point. Therefore, to assess the possibility of installing the antenna, it is necessary to collect meteorological data statistics, including temperature, humidity, and wind speed, using an autonomous weather station that needs to be installed there.

An experiment conducted in December 2013 showed a decrease in absorption at Mount Pastukhova (2733 m) by 13% or 0.3 mm PWV compared to the URS, with an altitude difference of about 700 m (Fig. 9, Bubnov et al., 2015). It is expected that on Semirodniki Hill, the average PWV values during the winter period will be lower by 0.10–0.15 mm, compared to the URS.

Table 2. Comparison of PWV values (mm) for different sites

Sites	Elevation, m	Fraction of time, %				
		90	50	25	10	5
NOEMA, winter	2550	7.0	2.1	1.0	0.3	0.2
NOEMA, total	2550	11.0	4.0	2.0	1.0	0.4
CARMA	2196	12.0	5.0	4.5	3.0	2.0
Zeiss-1000	2070	16.0	7.0	4.5	3.0	2.0
RATAN-600	974	20.0	11.5	7.5	4.5	3.5

4.4. Comparison of PWV at Some Locations

Typically, instruments operating in wavelengths shorter than 3 mm, are installed at high altitudes (ALMA, JCMT, LMA). However, there are telescopes that are located at altitudes below 3 km and successfully conduct observations at frequencies above 230 GHz. These include, for example, the 30-m telescope on Pico Veleta in Spain (IRAM30, 2850 m, Sánchez-Portal, 2023), the NOEMA interferometer (France, Southern Alps, 2550 m, Neri, 2016). It is also worth mentioning the CARMA instruments (Shiao et al., 2006, USA, 2196 m) and NMA (Japan, 1350 m, Morita, 1994), which operated for a long time at frequencies up to 300 GHz but were closed due to financial reasons as resources were redirected to the development of the ALMA project. Additionally, the e-KVN project (South Korea, Byun, 2021), is currently being prepared, proposing the installation of a 21-m antenna at an altitude of approximately 600 meters above sea level to operate at a frequency of 230 GHz.

Table 2 compares PWV values for different sites (CARMA, NOEMA, URS, and RATAN-600), showing the proportion of time that a PWV value less than the given one can be observed. From the provided estimates, it can be seen that the water content measured at Zeiss-1000 (URS) is quite comparable to the conditions at CARMA. It is expected that installing the antenna on Semirodniki Hill, which is 250 m higher, may slightly improve the PWV situation. As mentioned earlier, meteorological parameter monitoring is necessary at this location.

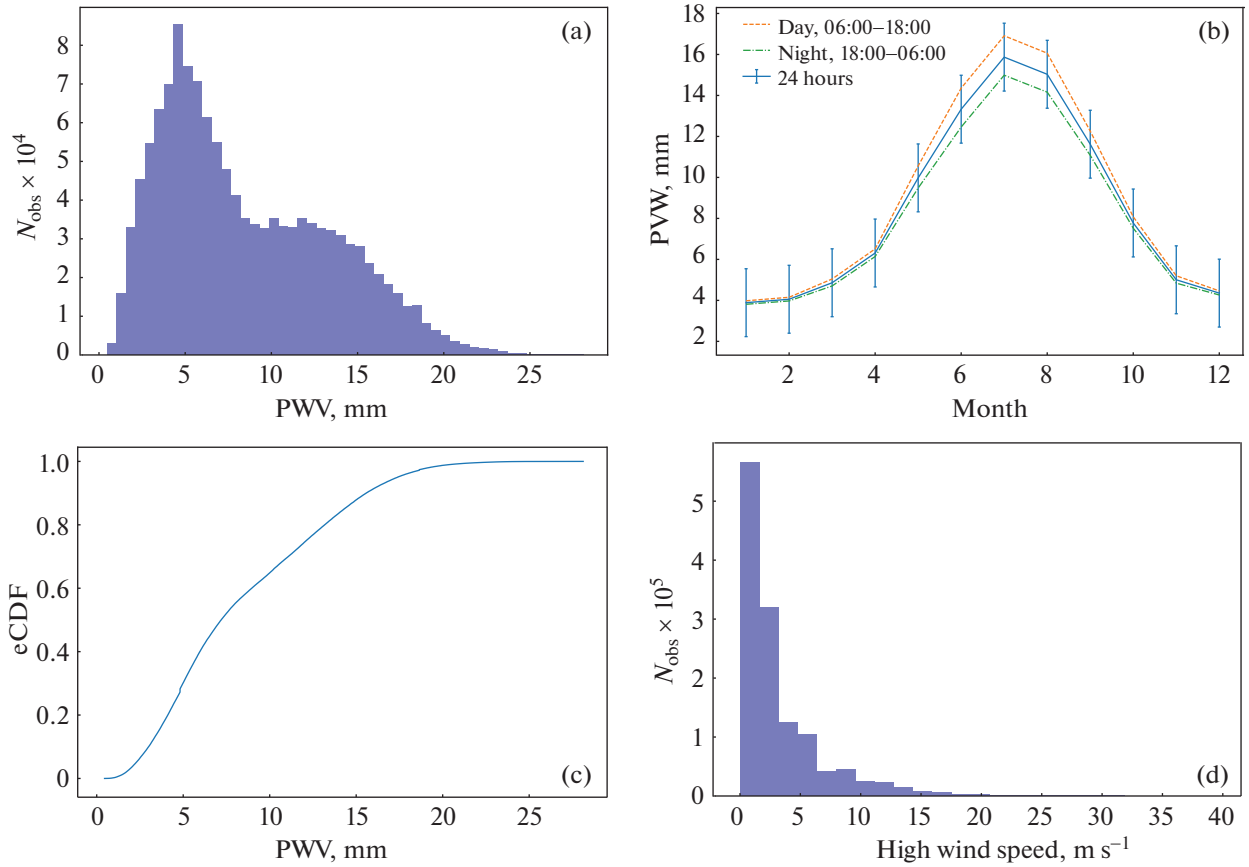

Fig. 5. Estimation of PWV at the Upper Research Site (Zeiss-1000) based on humidity and temperature values, as well as wind speed statistics for the period from 2008 to 2020. The panels depict: (a) the histogram distribution of PWV values; (b) averaged PWV values per month (daily, mean, nighttime); (c) cumulative probability distribution function (CDF) for PWV values; (d) histogram distribution of wind gust speeds.

5. SCIENTIFIC TASKS

In this section, some scientific problems that can be addressed with the proposed instrument operating in the millimeter band are listed.

It is worth noting that even in single-dish mode, entirely new tasks specific to this band can be addressed, which are novel to the SAO RAS. On the other hand, the interferometric mode implies extensive collaboration with other instruments, within which unique results can be obtained.

5.1. Single-Dish Mode

The primary operating mode of the millimeter telescope will be the single-dish mode. In Section 3.2, it was demonstrated that with half-hour integration time on the instrument, it will be possible to observe objects with a flux density of about 20 mJy with a signal-to-noise ratio of approximately $S/N \approx 5$. It should be noted that these estimates were made for a "typical" atmosphere with PWV around PWV $\approx$ 10 mm. Achieving such sensitivity opens up the possibility of observing both Galactic and a multitude of extragalactic objects. A simple extrapolation of the number of objects from the PCCS2 compact source catalog (Ade et al., 2016a) to the area with flux densities greater than 30 mJy yields an estimated number of available extragalactic sources of about 15–20 thousand at frequencies of 100–230 GHz.

Let us briefly consider the scientific tasks that can be addressed in single-dish mode.

5.1.1. CO line surveys and construction of maps of molecular line emission. Observations of rotational transitions of carbon monoxide molecules ^{12}CO $J = 1-0$ (115.27 GHz), ^{13}CO $J = 1-0$ (110.20 GHz) and ^{12}CO $J = 2-1$ (230.54 GHz) are used to detect the presence of molecular hydrogen H_2 in the interstellar medium, which is closely related to the process of star formation. Directly observing molecular hydrogen is challenging, so observations of CO molecular lines and the luminosity-to-mass ratio of CO to H_2 mass are used to determine the mass of H_2 in gas clouds (Shetty et al., 2011). Additionally, measurements of the Doppler shift of CO lines provide information about the object's kinematics.

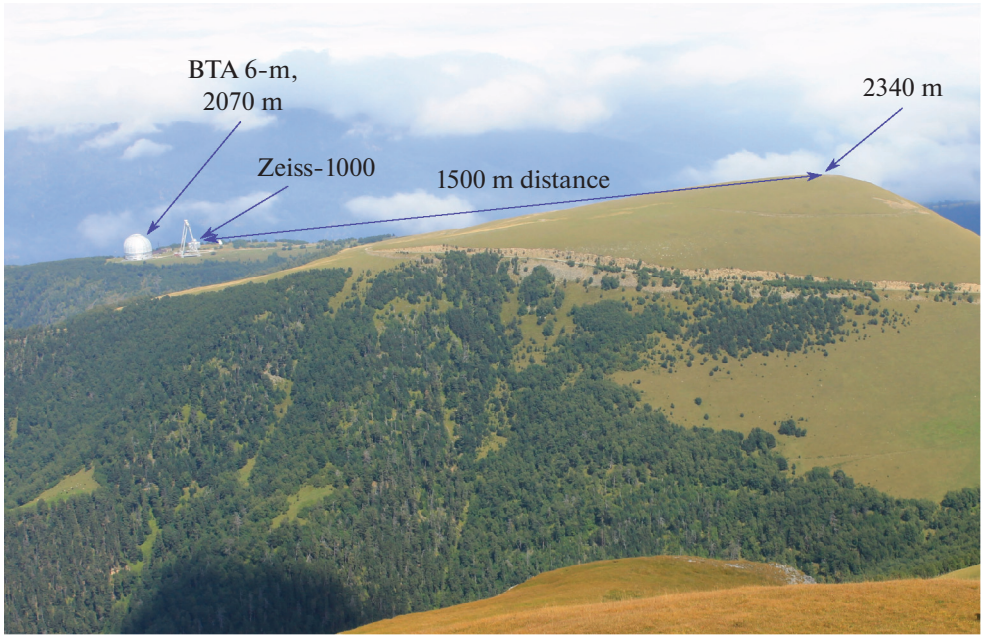

Fig. 6. Proposed location for installing the radio telescope on Semirodniki Hill.

Despite numerous CO line surveys conducted in recent years in our galaxy and neighboring galaxies, there are still many objects for which such data are lacking.

Additional information about the kinematics and chemical composition of molecular clouds can be obtained through observations of lines from other molecules, such as the aldehyde ion HCO^+ $J = 1-0$ (89.19 GHz), molecular ion N_2H^+ $J = 1-0$ (93.17 GHz), molecules CS (97.98 GHz), HCN (88.63 GHz), $C^{18}O$ (109.78 GHz) and many others (Lovas et al., 1979; Tzioumis, 2013).

5.1.2. Monitoring of active galactic nuclei. Using this instrument in a single-dish mode in conjunction with other ground-based radio telescopes, it will be possible to conduct quasi-simultaneous continuum measurements at frequencies up to 230 GHz for various subclasses of active galactic nuclei (AGN): blazars; Seyfert galaxies NLS 1; galaxies FR 0, FR I and FR II; compact young objects (CSS, GPS, HFP); extremely distant radio galaxies and quasars ($z > 3$). In addition to radio telescopes, instruments in other wavelength ranges, such as optical and gamma-ray instruments, are often involved in such monitoring programs (Bychkova et al., 2018). With the emergence of new efficient instruments, such as "Spectrum-RG" (Sunyaev et al., 2021), quasi-simultaneous monitoring programs across multiple wavelength bands will be particularly interesting, and the SAO RAS millimeter telescope can make a significant contribution to them.

Within such programs, studies of candidates for extragalactic sources of ultra-high-energy neutrinos (TeV–PeV), are possible, which will allow us to investigate the connection between neutrino events and radio flares in quasars, a relationship that has been statistically established (Plavin et al., 2020; Hovatta et al., 2021) and has been most pronounced at high radio frequencies—tens of GHz. Mass measurements of AGNs at hundreds of GHz will form the basis for the development of theories of efficient proton acceleration mechanisms in them.

The results of AGN monitoring programs can be used to calculate boundary conditions in the models of non-thermal emission mechanisms, estimate the conditions in the regions of gamma-ray emission genesis, and help to investigate the internal regions of relativistic jets at frequencies of hundreds of GHz, where synchrotron self-absorption is negligibly small.

5.1.3. Observations of the Sunyaev–Zeldovich effect in nearby galaxy clusters. The Sunyaev–Zeldovich (S–Z) thermal effect arises from the inverse Compton scattering of photons from the cosmic microwave background (CMB) radiation by electrons in the hot gas within galaxy clusters, leading to a change in the intensity of the CMB, which depends on the frequency (Sunyaev and Zeldovich, 1972). The deviations of the cosmic microwave background spectrum from the blackbody have a minimum at frequencies around 150 GHz, where a decrease in the CMB temperature is observed at the location of the galaxy cluster, and a maximum at frequencies around 400 GHz, where an increase in its temperature can be observed (see, for example,

Mroczkowski et al., 2019). At a frequency of around 220 GHz, the effect disappears.

S−Z effect has been observed using various instruments, notably the Planck space telescope, which provided observations used to construct a map of the comptonization parameter y for the entire celestial sphere and compile a catalog of galaxy clusters where this effect is observed (Ade et al., 2016b; Aghanim et al., 2016c). Among ground-based instruments, the S−Z effect has been observed using the South Pole Telescope (SPT) (Plagge et al., 2010; Everett et al., 2020) and the Atacama Cosmology Telescope (ACT) (Hilton et al., 2021), where measurements of surface brightness and gas pressure profiles have been made, and catalogs of galaxy clusters have been compiled. It should be noted that the angular resolution of Planck at frequencies of the HFI instrument ranging from 100 to 857 GHz varied from $10'.7$ to $5'.5$. The resolution of the SPT and ACT instruments at 150 GHz is $40''$ and $70''$.

Observations of the S−Z effect with the proposed instrument will be possible in the region of its minimum at 130–150 GHz (temperature decrement). Additionally, measurements at 220–230 GHz can be used to separate the S−Z effect from extraneous radiation, primarily the cosmic microwave background and thermal emission from dust. With a resolution of about $30''$ at 150 GHz, this instrument would offer comparable or even better spatial resolution than existing telescopes like the SPT, allowing for detailed studies of galaxy clusters in the northern celestial hemisphere.

Observations of the S−Z effect allow us to measure the gas pressure profile in the intergalactic medium, providing information about its thermodynamic structure. This includes insights into AGN feedback effects, global and turbulent motions, and the degree of asphericity in galaxy clusters.

By combining multi-frequency observations from different instruments, we can reconstruct the distribution of the electron temperature T_e in the cluster. This involves separating the contributions of various components and accounting for relativistic corrections to the S−Z effect (Chluba et al., 2013; Maillard et al., 2024). For this purpose, observations are needed both in the depression at 150 GHz, and in the maximum effect at 350 GHz. The proposed instrument would provide the necessary observational data in the required range for such joint data analysis.

Furthermore, X-ray observations provide direct information about the density and temperature of the gas in clusters, complementing other S−Z effect measurements. This comprehensive approach allows for a coherent understanding of the gas content in galaxy groups and clusters. Such joint analyses can be conducted with data from the "Spectr−RG," spacecraft, whose instruments have similar resolution capabilities (Sunyaev et al., 2021).

5.1.4. Building rotation curves of spiral galaxies and mapping dark matter. It has been noticed for quite some time that the rotation curves of spiral galaxies do not behave according to Kepler's law, as if they were composed solely of luminous matter (see, for example, Rubin et al., 1978). The outer regions of spiral galaxies rotate much faster than they should based on the estimated luminous mass, leading to the hypothesis that galaxies are embedded in a halo of dark matter. The nature of dark matter remains one of the key challenges in modern astrophysics (Zasov et al., 2017).

Usually, the kinematics of spiral galaxies, and particularly their rotation curves, are studied using observations of the neutral hydrogen H I line because the radial extent of the gas is much larger than the visible disk. In addition to this method, observations of molecular CO lines in the millimeter range are widely used to study the kinematics of the inner disk and central regions of spiral galaxies. This is because carbon monoxide typically has a higher concentration in these areas compared to neutral hydrogen H I, and also due to lower dust absorption (Sofue, 2017).

Furthermore, because of the much shorter wavelength of rotational transition emissions (for example, CO $J = 1-0$ has $\lambda = 2.6$ mm), significantly higher resolution can be achieved on a small instrument compared to observing the neutral hydrogen line at $\lambda = 21$ cm.

5.1.5. Continuum observations of objects within our Galaxy. The proposed millimeter telescope in this project can be used to observe the radio emission from X-ray binary systems in our Galaxy, known as microquasars. Microquasars are considered analogous to typical quasars but on stellar scales. They are tight X-ray binary systems where matter accretes from a companion–star onto a neutron star or a black hole. These systems exhibit activity in the radio spectrum due to relativistic jets. One of the typical representatives of this class of objects is GRS 1915+105 (Done et al., 2004).

Over the past 40 years, several dozen microquasars have been identified through X-ray observations, and ongoing radio monitoring of some of them is being conducted (Kim and Kim, 2004; Trushkin et al., 2017). However, these objects are primarily studied in the centimeter wavelength band, and additional data at millimeter wavelengths will allow for a more precise determination of their radio properties, such as spectral index, spectral energy distribution (SED), and their variations during outburst activity.

5.1.6. Observations of millimeter lines of complex molecules in the interstellar medium. The millimeter band is well-suited for observing

molecular lines of complex molecules, including organic ones. These molecules have been found not only in stellar atmospheres but also associated with dense and cold interstellar and circumstellar material. They are observed in small compact objects such as globules as well as in giant molecular clouds (GMCs). Molecules serve as indicators of the physical conditions in their environment and provide information about the lifetimes of their parent objects (Herbst and van Dishoeck, 2009).

By the present time, over 300 different molecules have been detected in the interstellar medium, with the majority being organic (McGuire, 2022). Many of these molecules, such as CH_3OH, C_2H_5OH, $(CH_3)_2O$, CH_3NH_2, which have simple structure, were discovered as far back as the 1970s. Complex organic molecules, such as glycolaldehyde (CH_2OHCHO) or aminoacetonitrile (NH_2CH_2CN) (a precursor to glycine NH_2CH_2COOH), have been discovered relatively recently (Ohishi, 2016).

Observations of interstellar molecules, including the search for prebiotic molecules, are crucial for understanding the chemical evolution of the Universe. With the frequency coverage of the proposed instrument reaching up to 230 GHz, it will be possible to measure a large number of molecular lines of complex molecules.

5.1.7. Studying star-forming regions in the Galaxy. It is believed that the stars are formed within dusty molecular clouds that are in a state of gravitational instability. Under the influence of gravity, the cloud fragments into regions of varying density, with denser formations becoming cores for the proto-objects.

Observing star-forming regions is most meaningful in wavelength bands where cloud absorption is minimal, particularly in the infrared and microwave spectra. The emission mechanism is associated with the re-emission of UV radiation from the stars by a dust in longer wavelengths, especially in the millimeter band.

To refine the chemical composition, which affects the cloud cooling process, and to study the kinematics, information provided by observations of molecular lines is necessary. With their help, other data about proto-objects can be obtained, such as gas temperature and concentration (Guilloteau, 2018).

Observing the dust component at frequencies of 100–300 GHz is an important part in studying the physical conditions in clouds where star formation occurs. By combining measurements in this range with higher-frequency observations near the peak of the dust emission spectrum, which follows a modified blackbody spectrum, one can determine the temperature of dust grains and make estimates of the cloud's mass.

5.1.8. Investigation of non-thermal solar radiation. The use of millimeter measurements together with centimeter measurements (ground-based instruments) will allow for a detailed study of the thermal structure of the chromosphere and the transition region to the corona in solar spots. Incorporating data from optical and UV bands will provide the opportunity to integrate the results into a comprehensive picture of the structure of the sunspot atmosphere from the lowest photospheric layers to coronal heights (Loukitcheva, 2019).

An instrument operating in the millimeter band can be used to study the heating processes of the solar corona and chromosphere. Despite significant progress made in recent decades, several fundamental questions regarding the structure and dynamics of the solar chromosphere remain unanswered. Among these questions is the issue of heating the chromosphere and corona, specifically, which mechanisms are responsible for heating and where it is localized. The presence of a whole class of objects such as recombination lines at short millimeter wavelengths opens up a new area of spectral studies of the solar chromosphere.

Millimeter radio astronomy offers a range of unique methods for estimating the magnetic field at chromospheric and transition region heights. As a result, it is possible to investigate the magnetic field structure in active regions and the small-scale features in the quiet Sun.

Among the potential tasks is the modification of the existing criterion for predicting proton events in solar plasma, understanding the mechanisms initiating them (Bogod et al., 2020), and investigating the nature of the sub-terahertz component of flare emissions.

It should be noted that observations of the Sun with instruments of this class are only possible with a specially designed antenna, such as those used with ALMA. There is a case described in the literature where the Sun accidentally entering the field of view of a millimeter telescope caused a fire on the secondary mirror (SEST, Leverington, 2016).

5.2. Using the Instrument as Part of the VLBI Network

The range of scientific tasks can be significantly expanded by incorporating the proposed millimeter band antenna into the VLBI network both at the national and international levels. Since there are plans to connect existing radio telescopes like RT-13 to the VLBI network in the future (see, for example, Ipatov, 2013; Kol'tsov et al., 2020), it would be beneficial to conduct modeling of such a network, which would

combine existing instruments (provided antenna surface improvements) with proposed instruments operating in the millimeter band.

Within the framework of preparing this article, modeling of observations of a multi-component source with a separation between components of several hundred microarcseconds was performed for various configurations of the VLBI network, including an antenna installed at the SAO RAS. For modeling the radio interferometer response, the `OSKAR`[10] software package was used, and image reconstruction, using the CLEAN method, was performed with the `WSClean`[11] program (Offringa et al., 2014). In this model, the central frequency was $\nu = 230$ GHz, $\Delta\nu = 1$ GHz, and the observation time was $t_{\rm obs} = 6^{\rm h}$. Errors in amplitude and phase were not modeled, assuming ideal calibrations, as the goal was to demonstrate the resolution limit of various VLBI network configurations and the impact of the number of antennas on the coverage of the uv-plane and, consequently, on the quality of the reconstructed image.

Figure 7 shows synthetic reconstructed images of a multi-component source with a minimum angular separation between components of 100 μas obtained from observations using two configurations of the millimeter-wave VLBI network. The first configuration includes the existing three RT-13 instruments (Svetloe, Zelenchukskaya, Badary), a millimeter antenna at the Upper Research Site (URS) of the SAO RAS, an antenna at the "Suffa" Radio Observatory and a millimeter instrument that may be constructed in the vicinity of Mount Shalbuzdag in Dagestan (Balega et al., 2022) or at another site in this region (Khaikin et al., 2022). This configuration can be considered as a national millimeter VLBI network.

The second configuration includes all six aforementioned antennas, plus four additional instruments that can be installed in China at sites identified as potentially suitable for millimeter observations by Tian et al. (2016)—Nanshan (Xinjiang), Ali (Tibet), Yangbajing (Tibet), and Delingha (Qinghai), provided that the existing antenna in Delingha is upgraded to operate at 1.3 mm (Yang et al., 2012).

The formal resolution of the VLBI network is determined by the maximum baseline, which in both cases is equal to the distance between the two most distant antennas (RT-13 Zelenchukskaya and RT-13 Badary, 4400 km, Shuygina et al., 2019), and at a frequency of 230 GHz is approximately 60 μas.

In the first configuration with six antennas, there are 15 baselines. The short baseline URS (SAO RAS)–RT-13 (Zelenchukskaya) provides sensitivity to large scales on the order of fractions of an arcsecond. Artifacts in the reconstructed CLEAN image in Fig. 7a are associated with the small number of baselines and insufficient coverage of the uv-plane. In the case of the second configuration with ten antennas, the resolution of the VLBI network is approximately the same (since the additional antennas are located west of the easternmost point in Badary), but with an increase in the number of baselines to 45 and a much denser coverage of the uv-plane, there is an obvious improvement in the quality of the reconstructed image (see Fig. 7b).

Since the projects for millimeter VLBI networks have been proposed earlier (see, for example, Asada et al., 2017), the objectives for such instruments have been articulated by various research groups. Below, we will briefly consider only some of them.

5.2.1. Compact extragalactic objects studies. When including a millimeter instrument in the VLBI network, it becomes possible to address a range of tasks requiring high angular resolution, such as:

- Investigating the radio emission and plasma dynamics in compact regions of AGN jets in VLBI mode;
- Studying the structure and formation processes of relativistic jets in AGN based on blazar monitoring data;
- Examining the morphology of compact young objects up to the epoch when they become radio-loud ($z > 6$).

Such programs could serve as important additions to the tasks mentioned above in single-dish mode. More detailed possibilities of millimeter VLBI networks in AGN observations are discussed by Boccardi et al. (2017).

5.2.2. Participation in the Event Horizon Telescope collaboration. The successful visualization of the shadow around the supermassive black hole in the core of the M87 galaxy by the Event Horizon Telescope (EHT) at 230 GHz (Fish et al., 2016) has opened a new era in direct experimental study of the geometry of spacetime in the Universe. The angular resolution of the EHT, approximately $\Delta\theta \simeq 20$ μas, is sufficient only for investigating the scale of the shadow radius. For the success of the EHT experiment, further measurements are needed, including those from the space-based millimeter interferometer network ("Millimetron"). The proposed instrument can provide an independent baseline for such an experiment to cover the uv-plane, for which there is currently no alternative.

5.2.3. Participation in VLBI network observations of maser emission sources. It is known that maser lines are associated with galactic and

[10] https://github.com/OxfordSKA/OSKAR
[11] https://gitlab.com/aroffringa/wsclean

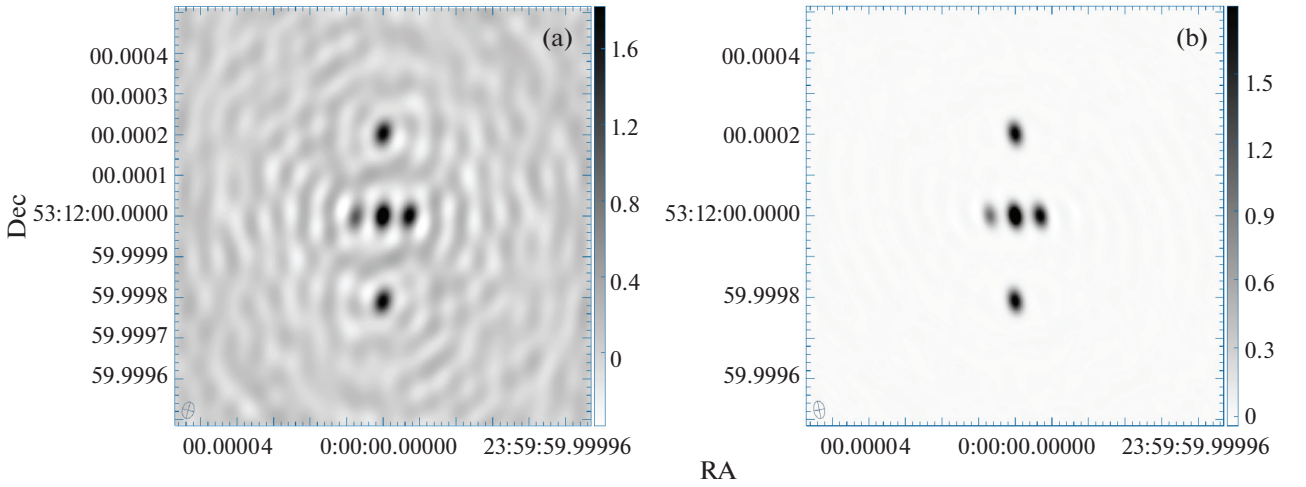

Fig. 7. Modeling observations of a multi-component object with angular separations ranging 100–300 μas between components in different configurations of the millimeter VLBI network: (a) 6 antennas; (b) 10 antennas.

extragalactic objects such as protostars, shock waves in star-forming regions and supernova remnants, circumstellar shells around AGB stars and red supergiants, as well as with gas disks around AGNs. Maser emission regions have compact structures with exceptionally high brightness temperatures (over 10^{10} K), making them ideal targets for VLBI observations. Maser sources in the millimeter and submillimeter bands are regularly observed by various instruments, including ALMA (Zinchenko et al., 2017). There are also reports of successful maser observations using a prototype of the millimeter VLBI network. For example, Shibata et al. (2004) published results of observing the SiO 86 GHz maser source in the circumstellar shell of the bright supergiant VY CMa, using two telescopes with a baseline length of approximately 1000 km.

A key feature of VLBI observations of masers is the ability to measure velocities in all three dimensions simultaneously, which can be achieved by observing the source at different epochs. By using the millimeter VLBI network, one can achieve a level of precision in determining the position and proper motion of the object that is an order of magnitude better than what can be obtained with conventional centimeter-range VLBI observations.

5.2.4. Collaboration on the "Millimetron" project. The space observatory "Millimetron" (Novikov et al., 2021) is a project of the Astro Space Center of Lebedev Physical Institute of the Russian Academy of Sciences (ASC LPI), within which a spacecraft with a 10-m antenna will be launched for observations in the wavelength range from 0.07 to 10 mm. It will implement both single-dish and "Earth–Space" interferometer mode.

The SAO RAS millimeter telescope can be used in the "Millimetron" project both for ground support (for monitoring target research objects) and as an additional station to create an independent base in the Northern Hemisphere, significantly improving the coverage of the space interferometer's uv-plane. The involvement of domestic scientific organizations such as the SAO RAS in this major international experiment will be a significant advantage.

5.2.5. The "Suffa" project. Within this project, it is planned to build a 70-m fully steerable antenna with a frequency range from 1 to 300 GHz on the Suffa plateau in Uzbekistan (Hojaev et al., 2007). To refine observation techniques and test receiving equipment, it would be beneficial to install additionally several small instruments with diameters of up to 15 meters both on the plateau in Uzbekistan and in the territory of Russia to create a VLBI network, which could include the millimeter-wave telescope of the Special Astrophysical Observatory of the Russian Academy of Sciences.

6. CONCLUSIONS

The article presents proposals for the development of the instrumental base in the millimeter wavelength band at the Special Astrophysical Observatory of the Russian Academy of Sciences.

Currently the SAO RAS, with the support of the Russian Science Foundation, is implementing a project for a subterahertz observatory as part of the BTA optical telescope. The project, which involves testing receiving equipment for the millimeter and submillimeter bands, is primarily aimed at demonstrating the possibility of observations in this wavelength band and serves as a "precursor" to a specialized instrument—a fully steerable antenna designed to address a range of scientific tasks.

The article discusses the possibility of creating and operating such a millimeter-wave telescope at the Upper Research Site of the SAO RAS. The tasks for this instrument are considered both for the single-dish mode and in collaboration with ground-based and space-based interferometers.

The authors are confident that the creation of a millimeter-wave telescope will be a significant step forward in the development of the astronomical instrumental base not only for the SAO RAS but also for the entire Russian astronomical community.

ACKNOWLEDGMENTS

Observations at the telescopes of the Special Astrophysical Observatory of the Russian Academy of Sciences are carried out with the support of the Ministry of Science and Higher Education of the Russian Federation. The update of the instrumental base is carried out within the framework of the national project "Science and Universities."

Manufacturing of samples of the investigated receiver structures of SIS (superconductor–insulator–superconductor) detectors is performed using equipment at the USF No. 352529 "Kriointegral."

Development and manufacturing of various electrical and mechanical interfaces for conducting research on receiver structures, as well as the development of the cryostatization system, are carried out based on the USF No. 3589084 "TSKP-7."

The authors are grateful to their colleagues N.V. Borisov, V.V. Vlasyuk, S.V. Drabek, M.A. Lukicheva, Yu.Yu. Kovalev and S.A. Trushkin for providing materials and fruitful discussions.

The authors thank the respected reviewers for their valuable comments and recommendations, which significantly improved this article.

FUNDING

The research was carried out with financial support from the Russian Science Foundation grant No. 23-62-10013 "Development of prototype for creation of a subterahertz observatory as part of an optical telescope."

CONFLICT OF INTEREST

The authors of this work declare that they have no conflicts of interest.

REFERENCES

1. R. Adam, A. Adane, P. A. R. Ade, et al., Astron. and Astrophys. **609**, id. A115 (2018). https://doi.org/10.1051/0004-6361/201731503
2. P. A. R. Ade et al. (Planck Collab.), Astron. and Astrophys. **594**, id. A26 (2016a). https://doi.org/10.1051/0004-6361/201526914
3. P. A. R. Ade et al. (Planck Collab.), Astron. and Astrophys. **594**, id. A27 (2016b). https://doi.org/10.1051/0004-6361/201525823
4. N. Aghanim et al. (Planck Collab.), Astron. and Astrophys. **594**, id. A22 (2016c). https://doi.org/10.1051/0004-6361/201525826
5. K. Akiyama et al. (Event Horizon Telescope Collaboration), Astrophys. J. **875** (1), article id. L2 (2019). https://doi.org/10.3847/2041-8213/ab0c96
6. K. Asada, M. Kino, M. Honma, et al., arXiv e-prints astro-ph:1705.04776 (2017). https://doi.org/10.48550/arXiv.1705.04776
7. Y. Balega, O. Bolshakov, A. Chernikov, et al., Photonics **10** (11), 1263 (2023). https://doi.org/10.3390/photonics10111263
8. Y. Balega, G. Bubnov, A. Chekushkin, et al., Sensors **24** (2), 359 (2024). https://doi.org/10.3390/s24020359
9. Y. Y. Balega, A. M. Baryshev, G. M. Bubnov, et al., Radiophysics and Quantum Electronics **63** (7), 479 (2020). https://doi.org/10.1007/s11141-021-10073-z
10. Y. Y. Balega, D. K. S. Bataev, G. M. Bubnov, et al., Doklady Physics **67** (1), 1 (2022). https://doi.org/10.1134/S1028335822010013
11. B. Boccardi, T. P. Krichbaum, E. Ros, and J. A. Zensus, Astron. Astrophys. Rev. **25** (1), article id. 4 (2017). https://doi.org/10.1007/s00159-017-0105-6
12. V. M. Bogod, T. I. Kal'tman, and M. A. Lukicheva, Geomagnetism and Aeronomy **59** (7), 783 (2020). https://doi.org/10.1134/S0016793219070077
13. G. M. Bubnov, E. B. Abashin, Y. Y. Balega, et al., IEEE Transactions on Terahertz Science and Technology **5** (1), 64 (2015). https://doi.org/10.1109/TTHZ.2014.2380473
14. V. S. Bychkova, A. E. Volvach, L. N. Volvach, et al., Astrophysical Bulletin **73** (3), 293 (2018). https://doi.org/10.1134/S1990341318030033
15. D.-Y. Byun, *13th East Asian VLBI Workshop 2021 (EAVW21)* (Chiang Mai, Thailand, 2021) (online at https://indico.narit.or.th/event/152/contributions/313/attachments/184/413/EAVW21-DoYoungByun.pdf).
16. J. Chluba, E. Switzer, K. Nelson, and D. Nagai, Monthly Notices Royal Astron. Soc. **430** (4), 3054

(2013).
https://doi.org/10.1093/mnras/stt110

17. Y. Chol Minh, H.-G. Kim, S.-T. Han, and D.-G. Roh, in *Proc. Intern. General Meeting VLBI Service for Geodesy and Astrometry, Ottawa, Canada, 2004*, Ed. by N. R. Vandenberg and K. D. Baver, NASA/CP-2004-212255, p. 156 (2004).
18. P. E. Dewdney, P. J. Hall, R. T. Schilizzi, and T. J. L. W. Lazio, Proceedings of the IEEE **97** (8), 1482 (2009).
https://doi.org/10.1109/JPROC.2009.2021005
19. C. Done, G. Wardziński, and M. Gierliński, Monthly Notices Royal Astron. Soc. **349** (2), 393 (2004).
https://doi.org/10.1111/j.1365-2966.2004.07545.x
20. S. Dougherty, *Abstracts of the 235th AAS Meeting*, **235**, id. 255.01 (2020).
21. V. S. Edelman, Instruments and Experimental Techniques **55** (1), 145 (2012).
https://doi.org/10.1134/S0020441212010277
22. H. Eklund, S. Wedemeyer, M. Szydlarski, et al., Astron. and Astrophys. **644**, id. A152 (2020).
https://doi.org/10.1051/0004-6361/202038250
23. W. B. Everett, L. Zhang, T. M. Crawford, et al., Astrophys. J. **900** (1), id. 55 (2020).
https://doi.org/10.3847/1538-4357/ab9df7
24. V. Fish, K. Akiyama, K. Bouman, et al., Galaxies **4** (4), id. 54 (2016).
https://doi.org/10.3390/galaxies4040054
25. M. Guélin and J. Cernicharo, Frontiers in Astronomy and Space Sciences **9**, id. 787567 (2022).
https://doi.org/10.3389/fspas.2022.787567
26. S. Guilloteau, Millimeter Astronomy, Saas-Fee Advanced Course **38**, 111 (2018).
https://doi.org/10.1007/978-3-662-57546-8_2
27. A. Gunbina, S. Mahashabde, M. Tarasov, et al., IEEE Transactions on Applied Superconductivity **31** (5), id. 3068999 (2021).
https://doi.org/10.1109/TASC.2021.3068999
28. A. Gunbina, M. Tarasov, M. Fominsky, et al., *Advances in Microelectronics: Reviews*, vol. 3 (IFSA Publishing, Barcelona, 2021), p. 183.
29. E. Herbst and E. F. van Dishoeck, Annual Rev. Astron. Astrophys. **47** (1), 427 (2009).
https://doi.org/10.1146/annurev-astro-082708-101654
30. M. Hilton, C. Sifón, S. Naess, et al., Astrophys. J. Suppl. **253** (1), article id. 3 (2021).
https://doi.org/10.3847/1538-4365/abd023
31. H. Hirabayashi, in *Proc. IAU Symp. No. 112*, Ed. by M. D. Papagiannis (D. Reidel Publishing Co., Dordrecht, 1985), p. 425.
32. A. Hojaev, G. I. Shanin, and Y. N. Artyomenko, in *Proc. IAU Meeting No. 26*, Ed. by J. B. Hearnshaw and P. Martinez (Cambridge University Press, Cambridge, 2007), p. 177.
https://doi.org/10.1017/S1743921307006965
33. T. Hovatta, E. Lindfors, S. Kiehlmann, et al., Astron. and Astrophys. **650**, id. A83 (2021).
https://doi.org/10.1051/0004-6361/202039481
34. D. H. Hughes, F. P. Schloerb, I. Aretxaga, et al., SPIE Conf. Proc. **11445**, id. 1144522 (2020).
https://doi.org/10.1117/12.2561893
35. B. T. Indermuehle and M. G. Burton, Publ. Astron. Soc. Australia **31**, id. e032 (2014).
https://doi.org/10.1017/pasa.2014.25
36. B. K. Ioannisiani, E. M. Neplokhov, I. M. Kopylov, et al., in *Proc. IAU Coll. No. 67*, Ed. by C. M. Humphries (D. Reidel Publishing Co., Dordrecht, 1982), p. 3.
https://doi.org/10.1007/978-94-009-7787-7_1
37. A. V. Ipatov, Physics—Uspekhi **56** (7), article id. 729 (2013).
https://doi.org/10.3367/UFNe.0183.201307i.0769
38. V. B. Khaikin, A. Y. Shikhovtsev, A. P. Mironov, and X. Qian, in *Proc. Conf. on Multifaceted Universe: Theory and Observations-2022, Nizhny Arkhyz, Spec. Astrophys. Obs. RAS, Russia, 2022*, id. 72 (2022) (online at https://pos.sissa.it/cgi-bin/reader/conf.cgi?confid=425).
https://doi.org/10.22323/1.425.0072
39. J.-S. Kim and S.-W. Kim, AIP Conf. Proc., **714**, 160 (2004).
https://doi.org/10.1063/1.1781020
40. N. Kol'tsov, S. Grenkov, and L. Fedotov, Journal of the Russian Universities. Radioelectronics **23** (2), 6 (2020).
https://doi.org/10.32603/1993-8985-2020-23-2-6-18
41. D. Kubo, C.-C. Han, H. Nishioka, et al., SPIE Conf. Proc. **10708**, id. 1070816 (2018).
https://doi.org/10.1117/12.2312241
42. S. Leclercq, https://www.iram.fr/ leclercq/Reports/About_NEP_photon_noise.pdf (2017).
43. D. Leverington, *Observatories and Telescopes of Modern Times* (Cambridge University Press, Cambridge, 2016).
https://doi.org/10.1017/9781139051507
44. M. Loukitcheva, Advances in Space Research **63** (4), 1396 (2019).
https://doi.org/10.1016/j.asr.2018.08.030
45. F. J. Lovas, D. R. Johnson, and L. E. Snyder, Astrophys. J. Suppl. **41**, 451 (1979).
https://doi.org/10.1086/190626
46. J. Magnum, https://library.nrao.edu/public/memos/alma/main/memo602.pdf (2017).

47. J. P. Maillard, A. Mihalchenko, D. Novikov, et al., Phys. Rev. D **109** (2), article id. 023523 (2024). https://doi.org/10.1103/PhysRevD.109.023523
48. B. A. McGuire, Astrophys. J. Suppl. **259** (2), id. 30 (2022). https://doi.org/10.3847/1538-4365/ac2a48
49. K.-I. Morita, ASP Conf.Ser. **59** 18 (1994).
50. T. Mroczkowski, D. Nagai, K. Basu, et al., Space Science Reviews **215** (1), article id. 17 (2019). https://doi.org/10.1007/s11214-019-0581-2
51. R. Neri, in *9th IRAM Millimeter Interferometry School, Grenoble, 2016* (online at https://web-archives.iram.fr/IS/IS2016/presentations/neri-noema.pdf).
52. I. D. Novikov, S. F. Likhachev, Y. A. Shchekinov, et al., Physics—Uspekhi **64** (4), 386 (2021). https://doi.org/10.3367/UFNe.2020.12.038898
53. A. R. Offringa, B. McKinley, N. Hurley-Walker, et al., Monthly Notices Royal Astron. Soc. **444** (1), 606 (2014). https://doi.org/10.1093/mnras/stu1368
54. M. Ohishi, *Journal of Physics: Conference Series*, vol. 728, article id. 052002 (2016). https://doi.org/10.1088/1742-6596/728/5/052002
55. A. Otárola, T. Travouillon, M. Schöck, et al., Publ. Astron. Soc. Pacific **122** (890), 470 (2010). https://doi.org/10.1086/651582
56. Y. N. Parijskij, IEEE Antennas and Propagation Magazine **35**, 7 (1993). https://doi.org/10.1109/74.229840
57. A. Pellegrini, J. Flygare, I. P. Theron, et al., IEEE Journal of Microwaves **1** (1), 428 (2021). https://doi.org/10.1109/JMW.2020.3034029
58. T. Plagge, B. A. Benson, P. A. R. Ade, et al., Astrophys. J. **716** (2), 1118 (2010). https://doi.org/10.1088/0004-637X/716/2/1118
59. A. Plavin, Y. Y. Kovalev, Y. A. Kovalev, and S. Troitsky, Astrophys. J. **894** (2), id. 101 (2020). https://doi.org/10.3847/1538-4357/ab86bd
60. I. Prandoni, M. Murgia, A. Tarchi, et al., Astron. and Astrophys. **608**, id. A40 (2017). https://doi.org/10.1051/0004-6361/201630243
61. V. C. Rubin, W. K. Ford Jr., and N. Thonnard, Astrophys. J. **225**, L107 (1978). https://doi.org/10.1086/182804
62. K. I. Rudakov, P. N. Dmitriev, A. M. Baryshev, et al., Radiophysics and Quantum Electronics **62** (7–8), 547 (2020). https://doi.org/10.1007/s11141-020-10001-7
63. M. Sánchez-Portal, in *Proc. Scientific Meeting of the Spanish Astronomical Society, La Laguna, Spain, 2022*, Ed. by M. Manteiga, L. Bellot, P. Benavidez, A. de de Lorenzo-Cáceres, M. A. Fuente, M. J. Martínez, M. Vázquez Acosta, C. Dafonte (online at https://zenodo.org/records/7047921#.Y78DgOzMKek), 2023.
64. K. F. Schuster, R. Neri, F. Gueth, et al., SPIE Conf. Proc. **10700**, p. 107000R (2018). https://doi.org/10.1117/12.2313489
65. R. Shetty, S. C. Glover, C. P. Dullemond, and R. S. Klessen, Monthly Notices Royal Astron. Soc. **412** (3), 1686 (2011). https://doi.org/10.1111/j.1365-2966.2010.18005.x
66. Y.-S. Shiao, L. W. Looney, D. P. Woody, et al., SPIE Conf. Proc. **6275**, id. 62750Y (2006). https://doi.org/10.1117/12.672245
67. K. M. Shibata, H.-S. Chung, S. Kameno, et al., Publ. Astron. Soc. Japan **56**, 475 (2004). https://doi.org/10.1093/pasj/56.3.475
68. N. Shuygina, D. Ivanov, A. Ipatov, et al., Geodesy and Geodynamics **10** (2), 150 (2019). https://doi.org/10.1016/j.geog.2018.09.008
69. Y. Sofue, Publ. Astron. Soc. Japan **69** (1), id. R1 (2017). https://doi.org/10.1093/pasj/psw103
70. R. Sunyaev, V. Arefiev, V. Babyshkin, et al., Astron. and Astrophys. **656**, id. A132 (2021). https://doi.org/10.1051/0004-6361/202141179
71. R. A. Sunyaev and Y. B. Zeldovich, Comments on Astrophysics and Space Physics **4**, 173 (1972).
72. M. Tarasov, A. Gunbina, A. Chekushkin, et al., Applied Sciences **11** (20) id. 9649 (2021). https://doi.org/10.3390/app11209649
73. M. Tarasov, A. Gunbina, A. Chekushkin, et al., Applied Sciences **12** (20), id. 10525 (2022). https://doi.org/10.3390/app122010525
74. M. A. Tarasov, A. A. Gunbina, S. Mahashabde, et al., IEEE Transactions on Applied Superconductivity **30** (3), id. 2941857 (2020). https://doi.org/10.1109/TASC.2019.2941857
75. J. F. Tian, L. C. Deng, X. B. Zhang, et al., Publ. Astron. Soc. Pacific **128** (968), 105003 (2016). https://doi.org/10.1088/1538-3873/128/968/105003
76. S. Trushkin, N. Nizhelskij, P. Tsybulev, and G. Zhekanis, Galaxies **5** (4), id. 84 (2017). https://doi.org/10.3390/galaxies5040084
77. A. Tzioumis, Handbook on Radio Astronomy (2013) on-line at http://handle.itu.int/ 11.1002/pub/809847c8-en.
78. A. N. Vystavkin, A. G. Kovalenko, S. V. Shitov, et al., SPIE Conf. Proc. **7020**, article id. 702024 (2008). https://doi.org/10.1117/12.788744
79. A. N. Vystavkin, S. V. Shitov, S. E. Bankov, et al., Radiophysics and Quantum Electronics **50** (10-11), 852 (2007). https://doi.org/10.1007/s11141-007-0077-x

80. T. L. Wilson and S. Guilloteau, *Millimeter Astronomy* (Springer, Berlin, 2018). https://doi.org/10.1007/978-3-662-57546-8
81. P. Yagoubov, T. Mroczkowski, V. Belitsky, et al., Astron. and Astrophys. **634**, id. A46 (2020). https://doi.org/10.1051/0004-6361/201936777
82. D. Yang, Y. Zhang, G. Zhou, et al., SPIE Conf. Proc. **8444**, article id. 84444B (2012). https://doi.org/10.1117/12.925789
83. R. A. Yusupov, A. A. Gunbina, A. M. Chekushkin, et al., Physics of the Solid State **62** (9), 1567 (2020). https://doi.org/10.1134/S106378342009036X
84. A. V. Zasov, A. S. Saburova, A. V. Khoperskov, and S. A. Khoperskov, Physics–Uspekhi **60** (1), 3 (2017). https://doi.org/10.3367/UFNe.2016.03.037751
85. I. Zinchenko, S. Y. Liu, Y. N. Su, and A. M. Sobolev, Astron. and Astrophys. **606**, id. L6 (2017). https://doi.org/10.1051/0004-6361/201731752

Translated by E. Porfiryeva